Spectral method to compute mesoscale mass-consistent wind fields on a complex terrain

Marco A. Núñez, Jorge E. Sánchez−Sánchez

Departamento de Física, Universidad Autónoma Metropolitana Iztapalapa,
A. P. 55-534, C.P. 09340, D. F., México. e-mail: manp@xanum.uam.mx

1. Introduction

One of the main physical constraints that wind field has to satisfy, is the conservation of mass [1,2]. Several methods have been proposed to get mass-consistent wind fields from a data set provided by a meteorological network of numerical solutions of the hydrodynamic equations. These methods go from a simple interpolation to the numerical solution of primitive-equation models in 3D or 4D data-assimilation schemes [3]. The class of Variational Mass consistent models (VMCM's) of the wind field, belongs to a class of diagnostic models that is intermediate in sophistication between interpolated and primitive-equation models and attempts to satisfy the continuity equation [2-6]. Several studies give evidence that these models appear to be suitable for several applications since they introduce a fewer number of arbitrary parameters [5-7]. VMCM's have been applied to model the transport, diffusion and dispersion of atmospheric pollutants and as input of prognostic models [5-13], a review of these models is given in Refs. [5,6]. The simplicity of VMCM's has motivated the development of new computational algorithms [11-15] and applications for air quality modeling and climatological studies [12,16,17] over the last decades.

The main aim of this work is to propose a scheme to compute VMCM's. The scheme has the following features: (i) The formulation uses a functional in the space of contravariant vector fields that leads to an elliptic equation which can be solved explicitly by means of eigenfunction expansions independently of the complexity of the terrain. This reduces the computational problem to the use of 2D and 3D Fast Fourier Algorithm (FFT), for which there are highly efficient computational routines. (ii) The scheme yields an explicit expression of the accuracy of the wind field to satisfy the continuity equation, expression that requires only the estimation of a three-dimensional Fourier Series. (iii) The imposed boundary conditions are easy to use and improve in several orders of magnitude the accuracy with which velocity field satisfies the continuity equation. The method is illustrated by numerical examples. Preliminary formal results of our approach are found in [18].

2. The proposal

Our proposal considers a bounded region Ω_σ in computational space $\sigma^1\sigma^2\sigma^3 = xy\sigma$ with boundary Γ_σ. Let Γ be the image of Γ_σ when the cartesian coordinates transformation equations are given by

$$x^i = x^i(\sigma^j)\ . \tag{2.1}$$

If $\mathbf{n}$ is the outward unit normal to Γ and $\mathbf{v}_{\mathrm{T}}$ denotes the true velocity field it is natural to consider the estimation of a velocity field with the physical constraint

$$\mathbf{n}\cdot\mathbf{v} = \mathbf{n}\cdot\mathbf{v}_{\mathrm{T}} \quad \text{on the whole boundary } \Gamma\ . \tag{2.2}$$

The formulation to get a VMCM from an initial field $\mathbf{v}^0$ in Ω_σ, is as follows. For a given symmetric and positive–definite matrix $\mathbb{S} = \{S_{ij}\}$, we want to find the field $\mathbf{v}$ whose contravariant form $\mathbf{v}^\eta$ minimizes the functional

$$J(\mathbf{v}^\eta) = \int_{\Omega_\sigma} (\mathbf{v}^\eta - \mathbf{v}^{0\eta})\cdot\mathbb{S}(\mathbf{v}^\eta - \mathbf{v}^{0\eta}) d\Omega_\sigma \tag{2.3}$$

subject to the constraint $\boldsymbol{\nabla}\cdot\mathbf{v}=0$ and (2.2). The field $\mathbf{v}^{\eta}$ is unique and given by

$$\mathbf{v}^{\eta}=\mathbf{v}^{0\eta}+\sqrt{g}\mathbb{S}^{-1}\nabla_{\sigma}\lambda\ . \tag{2.4}$$

where $\sqrt{g}$ is the Jacobian of transformation equations (2.1). The constraints imply that λ is solution of the elliptic problem

$$L\lambda=\sqrt{g}\nabla\cdot\mathbf{v}^{0}\quad\text{ in }\Omega_{\sigma},\qquad \mathcal{L}\lambda=\mathbf{n}_{\sigma}\cdot(\mathbf{v}_{\mathrm{T}}^{\eta}-\mathbf{v}^{0\eta})\qquad\text{on }\Gamma_{\sigma}\ , \tag{2.5}$$

where we set $L\equiv-\nabla_{\sigma}\cdot g\mathbb{S}^{-1}\nabla_{\sigma}$, $\mathcal{L}=\mathbf{n}_{\sigma}\cdot\sqrt{g}\mathbb{S}^{-1}\nabla_{\sigma}$. To get a practical form of problem (2.5) we consider: (i) A diagonal matrix $\mathbb{S}$ with elements $S_{11}=S_{22}=1$, with constant $S_3\equiv S_{33}$, (ii) the domain

$$\Omega_{\sigma}=\Omega_{xy}\times(0,\sigma_{M})\ ,\ \ \Omega_{xy}=(0,x_{M})\times(0,y_{M})\ ,$$

and (iii) the coordinate $\sigma=z-h\,(x,y)$ where $h\,(x,y)$ denotes the terrain elevation with respect to the xy plane.

The boundary condition (2.2) is estimated as follows. In meteorology and oceanography, where the vertical velocity is not measured by operational networks, the interpolation of data with standard methods will yield an initial field of the form

$$\mathbf{v}^{0}=u^{0}\mathbf{i}+v^{0}\mathbf{j}\ . \tag{2.6}$$

This field yields the simplest mass-consistent field

$$\mathbf{U}^{0}=\mathbf{v}^{0}+w^{0}\mathbf{k} \tag{2.7a}$$

where the vertical velocity w^{0} is determined by the problem

$$\nabla\cdot\mathbf{U}^{0}=0\text{ in }\Omega\quad\text{ subject to }\ \mathbf{U}^{0}\cdot\mathbf{n}=0\ \text{ on }\sigma=0\ , \tag{2.7b}$$

where we have assumed σ satisfies that $\sigma(x,y,z)=0$ holds for $z=h\,(x,y)$. The solution is

$$w^{0}=h_{x}u^{0}+h_{y}v^{0}-\int_{0}^{\sigma}(\partial_{x}u^{0}+\partial_{y}v^{0})ds\ . \tag{2.7c}$$

Thus we get the problem

$$L\lambda=\nabla\cdot\mathbf{v}^{0}\quad\text{ in }\Omega_{\sigma},\qquad \mathcal{L}\lambda=\mathbf{n}_{\sigma}\cdot(\mathbf{U}^{0\eta}-\mathbf{v}^{0\eta})\qquad\text{on }\Gamma_{\sigma}\ , \tag{2.8}$$

For computational purposes, problem (2.8) is replaced by the approximated one

$$L\lambda_{mn}=F_{mn}\quad\text{ in }\Omega_{\sigma},\qquad \mathcal{L}\lambda_{mn}=\xi_{mn}\ \text{ on }\Gamma_{\sigma}\ , \tag{2.9}$$

where λ_{mn}, F_{mn}, ξ_{mn}, are Fourier series of λ, $F\equiv\nabla\cdot\mathbf{v}^{0}$, $\mathbf{n}_{\sigma}\cdot(\mathbf{U}^{0\eta}-\mathbf{v}^{0\eta})$ on Γ_{σ}, with the eigenfunctions of $-\partial_{x}^{2}$, $-\partial_{y}^{2}$, subject to Neumann boundary conditions. The eigenfunctions are

$$\begin{aligned}\phi_{i=0}&=1/\sqrt{x_{M}},\quad \phi_{i\geq1}=\sqrt{2/x_{M}}\cos\omega_{i}x,\quad \omega_{i}=i\pi/x_{M}\ ,\\ \phi_{j=0}&=1/\sqrt{y_{M}},\quad \phi_{j\geq1}=\sqrt{2/y_{M}}\cos\omega_{j}y,\quad \omega_{j}=j\pi/y_{M}\ .\end{aligned}$$

The dependence of λ_{mn} in σ is computed by means of Green's functions. Detailed expressions are given in [18,19]. The corresponding field $\mathbf{v}_{mn}$ has the contravariant form

$$\mathbf{v}_{mn}^{\eta}=\mathbf{v}_{mn}^{0\eta}+\mathbb{S}^{-1}\nabla_{\sigma}\lambda_{mn}\ , \tag{2.10}$$

and its divergence is given by

$$\nabla\cdot\mathbf{v}_{mn}=F-F_{mn}\ . \tag{2.11}$$

An important feature of $\mathbf{v}_{mn}$ is that it allows us to recover $\mathbf{U}^0$ by means of the limiting procedure

$$\lim_{S_3 \to 0} \mathbf{v}_{mn} = \mathbf{U}^0_{mn} \tag{2.12}$$

where $\mathbf{U}^0_{mn}$ is the corresponding Fourier series of $\mathbf{U}^0$.

3. Examples

In this section we give some examples with a nontrivial topographic surface $h(x, y)$. The streamlines of $\mathbf{v}_{mn}$ are computed with the fourth-order Runge-Kutta method.

Example 1. Consider a constant field

$$\mathbf{v}^0 = u^0\mathbf{i} + v^0\mathbf{j} \tag{3.1}$$

and the topographic surface

$$h = 0.2\,[1 + \cos(\omega_h x)\cos(\omega_h y)] \quad \text{with} \quad \omega_h = 4\pi/x_M\ . \tag{3.2}$$

We have $\nabla \cdot \mathbf{v}^0 = 0$ but $\mathbf{v}^0$ does not satisfy BC $\mathbf{v}^0 \cdot \mathbf{n} = 0$ on $z = h$. This yields $\nabla \cdot \mathbf{v}_{mn} = 0$ for all m, n, the product mn determines the accuracy with which $\mathbf{v}_{mn}$ satisfies $\mathbf{n} \cdot \mathbf{v}_{mn} = 0$ on $z = h$. The field $\mathbf{v}_{m=n=32}$ is computed in a domain Ω_σ with $x_M = y_M = 10$ km, $\sigma_M = 5$ km, $u^0 = v^0 = 0.3$ ms^{-1}. Figure 1 shows the resulting streamlines of $\mathbf{v}^0$, $\mathbf{v}_{mn}$.

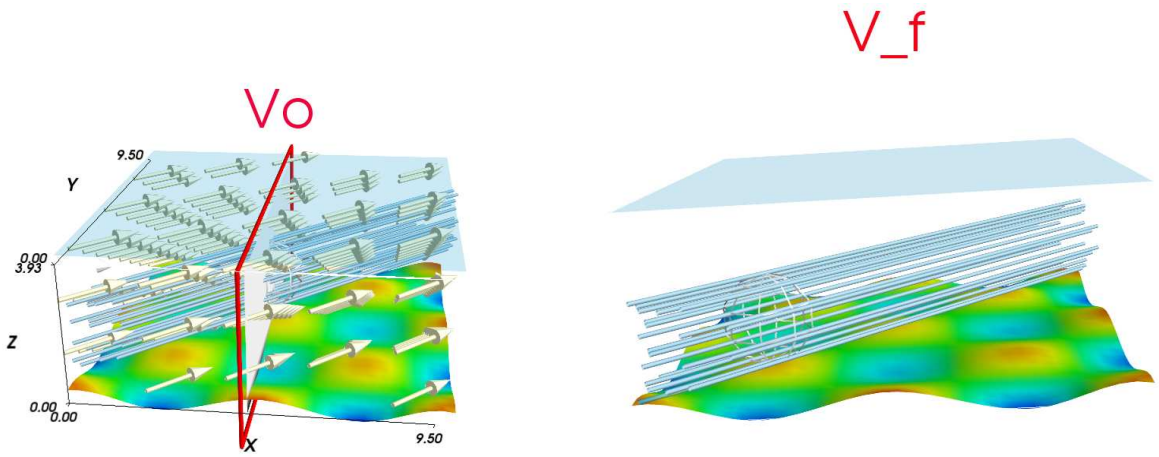

(a) **(b)**

Figure 1: a). The initial $\mathbf{v}^0$ field: $\mathbf{v}^0 = 0.3\mathbf{i} + 0.3\mathbf{j}$, over a terrain $h = 0.2\,[1 + \cos(1.26x)\cos(1.26y)]$, scale is in km, colors in the perpendicular plane (framed in red) show the magnitud of the vector field at the given position, some current lines are shown in clear blue color. b). The resulting mass conservative $\mathbf{v}^f$ current lines, for the case in a) shown in clear blue color. The discretized mesh being 32x32x6, with 6144 nodes in total.

Example 2. Consider

$$\mathbf{v}^0 = \beta x\mathbf{i} + \beta y\mathbf{j}$$

with $\beta = 0.06$ s^{-1}. We have $F = F_{mn}$, $\nabla \cdot \mathbf{v}_{mn} = 0$ for n, $m \geq 1$, mn determines the accuracy with which $\mathbf{v}_{mn}$ is tangent to the terrain. The field $\mathbf{v}_{m=n=32}$ is computed in a domain Ω_σ with $x_M = y_M = 10$ km, $\sigma_M = 5$ km, and terrain h (3.2). Figure 2 shows the streamlines of $\mathbf{v}^0$, $\mathbf{v}_{mn}$.

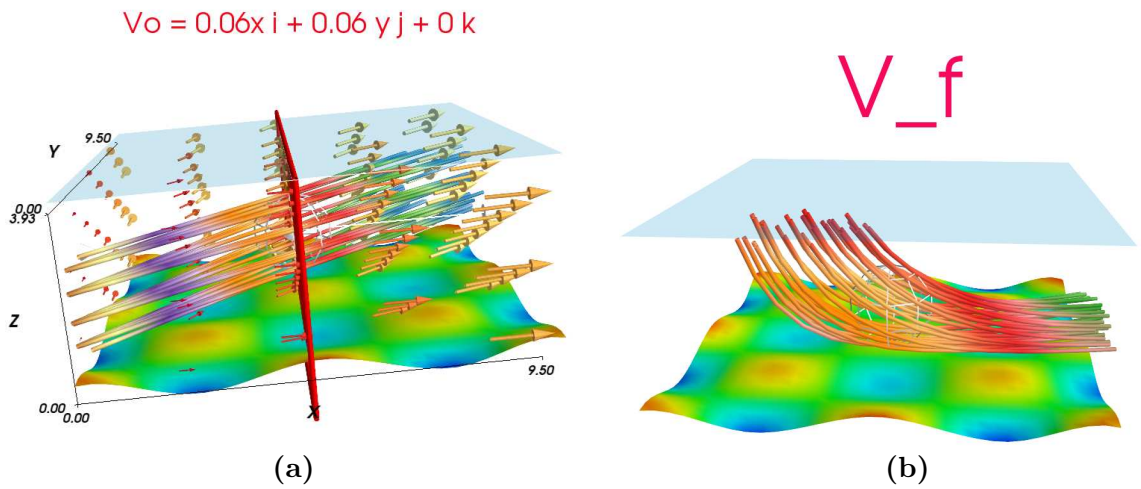

(a) **(b)**

Figure 2: a). The initial $\mathbf{v}^0$ field: $\mathbf{v}^0 = 0.06x\mathbf{i} + 0.06y\mathbf{j}$, over a terrain $h = 0.2\,[1 + \cos(1.26x)\cos(1.26y)]$, scale is in km, some current lines are shown passing near the center of the domain. b). The resulting mass conservative $\mathbf{v}^f$ current lines, for the case in a).The discretized mesh being 32x32x6, with 6144 nodes in total.

Example 3. Consider an oscillating field

$$\mathbf{v}^0 = \beta \sin(wx)\mathbf{i} + \beta \sin(wy)\mathbf{j}$$

with $\beta = 0.1$ s^{-1}, $w = 0.6\pi$, and the topographic surface h (3.2). The field $\mathbf{v}_{m=n=64}$ is computed in a domain Ω_σ with $x_M = y_M = 10$ km, $\sigma_M = 5$ km. Figure 3 shows some resulting streamlines of $\mathbf{v}_{mn}$.

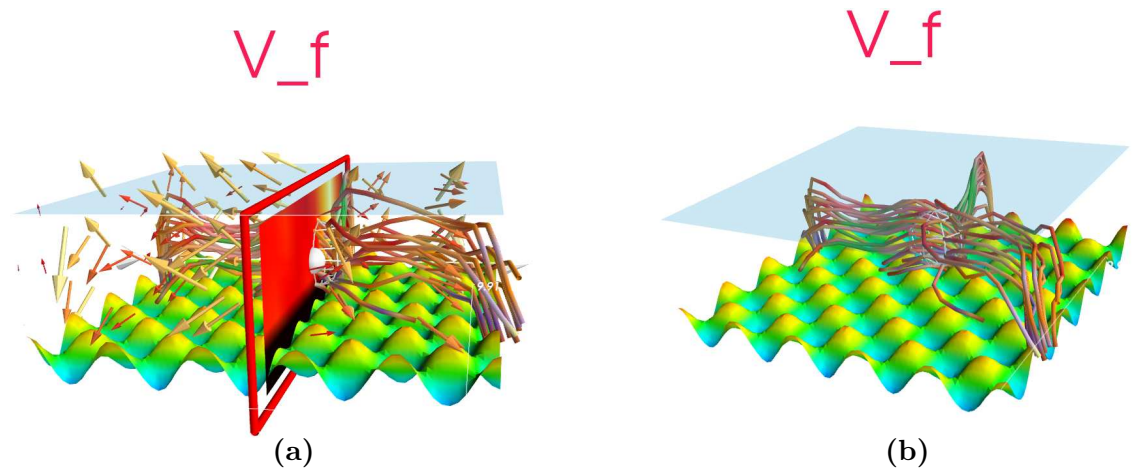

(a) **(b)**

Figure 3: a). Two sets of current lines of the resulting mass conservative field $\mathbf{v}^f$, for the Example 3. The discretized mesh being 64x64x6, with 24576 nodes in total.

Example 4. Consider the previous oscillating field multiplied by an exponential decaying with height term

$$\mathbf{v}^0 = \beta \exp(-\sigma/\sigma_M)(\sin(wx)\mathbf{i} + \sin(wy)\mathbf{j})$$

with $\beta = 0.1$ s^{-1}, $\sigma_M = 5$ km, $w = 0.6\pi$, and the topographic surface h (3.2). The field $\mathbf{v}_{m=n=64}$ is computed in a domain Ω_σ with $x_M = y_M = 10$ km, $\sigma_M = 5$ km. Figure 4 shows resulting streamlines of $\mathbf{v}_{mn}$ passing through the middle of the domain.

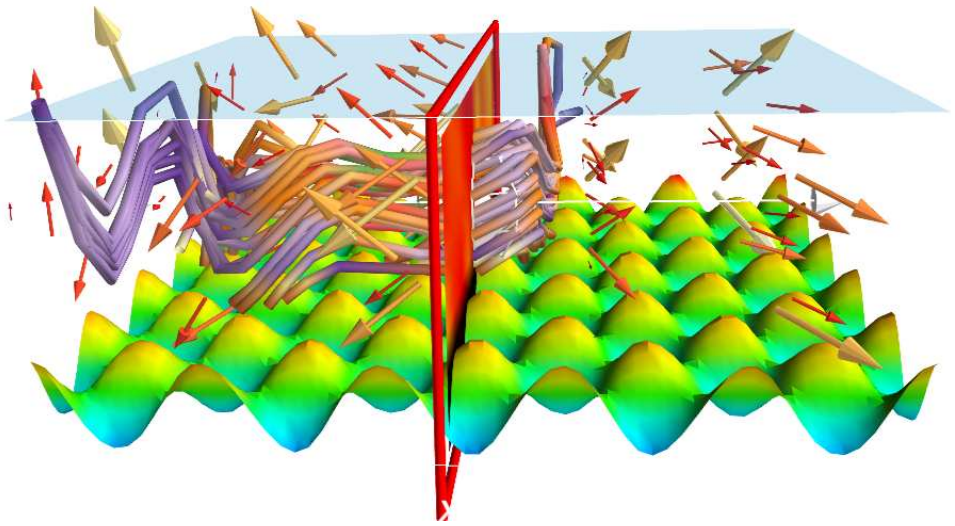

Figure 4: Current lines of the resulting mass conservative field $\mathbf{v}^f$, for the Example 4. The discretized mesh being 64x64x6, with 24576 nodes in total.

Our next example considers as the topography $h(x, y)$ an interpolated region of 40km $\times$ 40km of the valley of Mexico's City shown in Figure 5.

Example 5. Consider the field $\mathbf{v}^0$ of Example 4. Figure 6 shows the streamlines of $\mathbf{v}^0$, $\mathbf{v}_{mn}$, over the top of the Ajusco mountain in Mexico City.

4. Limitations of kinematic method to compute vertical velocity

Since the vertical velocity is not measured directly by operational networks, it has to be estimated. A standard method to compute the vertical velocity from a field $\mathbf{v}^0 = u^0\mathbf{i} + v^0\mathbf{j}$ obtained by interpolation of data, is based on the integration of the continuity equation. This is the so-called *kinematic method* [20] which consists in computing $\mathbf{U}^0 = \mathbf{v}^0 + w^0\mathbf{k}$ by solving problem (2.7b), which yields the vertical velocity (2.7c). However, we have the following result: *The field* $\mathbf{U}^0$ *may have an unphysical behavior.* To show this consider the field

$$\mathbf{v}^0 = u^0(x, y)\mathbf{i} + v^0(x, y)\mathbf{j} \ . \tag{4.1}$$

Let $\tilde{x}(t, x_0, y_0)$, $\tilde{y}(t, x_0, y_0)$, be the solution of the initial value problem

$$\dot{x} = u^0(x, y), \qquad \dot{y} = v^0(x, y) \ . \tag{4.2}$$

with initial conditions x_0, y_0. Replacing $\tilde{x}$, $\tilde{y}$, into equation

$$\dot{z} = w^0\left[x, y, \sigma(x, y, z)\right] = h_x u^0 + h_y v^0 - \int_0^\sigma (\partial_x u^0 + \partial_y v^0) ds \tag{4.3}$$

and solving it with $z(0) = z_0 \geqslant h(x_0, y_0)$, we get $z = z(t, x_0, y_0, z_0)$. Thus the streamlines of $\mathbf{U}^0$ have the vector form

$$\mathbf{R}(t, z, x_0, y_0) = \mathbf{r}_{xy}(t, x_0, y_0) + z\mathbf{k} \ , \ \ \mathbf{r}_{xy} = \tilde{x}\mathbf{i} + \tilde{y}\mathbf{j} \ . \tag{4.4}$$

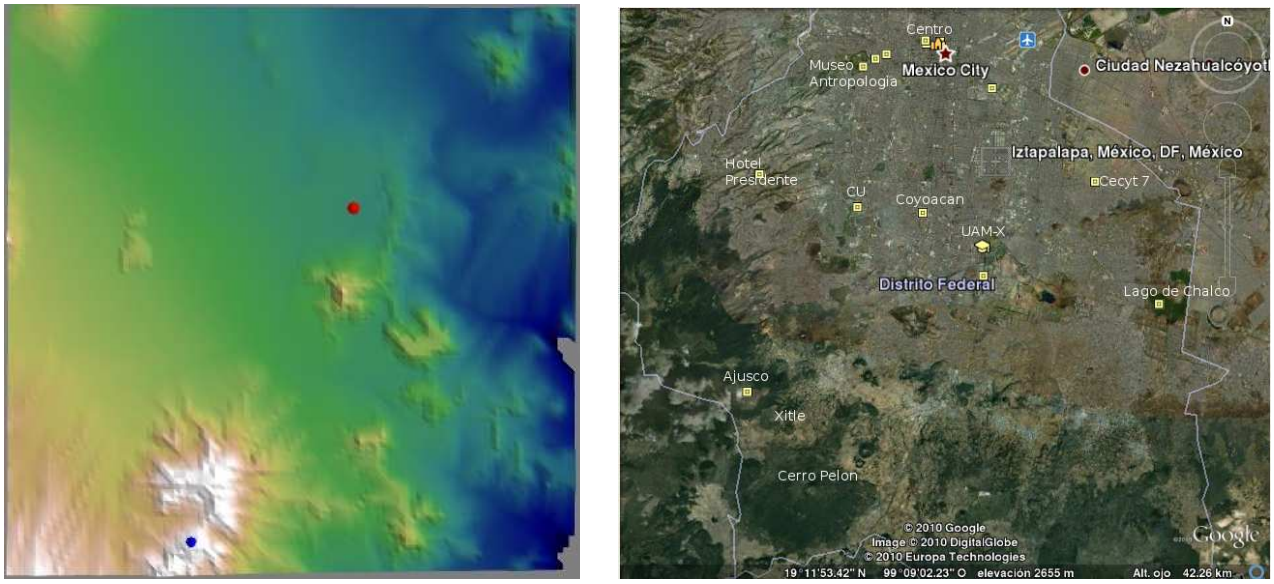

(a) **(b)**

Figure 5: a). The interpolated topography of Mexico City. b). Google Earth image for ubication reference.

which is the vectorial equation of a cylindrical surface $\mathcal{S}_h$ generated by moving vertically the curve $\mathbf{r}_{xy}(t, x_0, y_0)$ on $xy-$plane. Therefore, the streamlines of $\mathbf{U}^0$ belong the surface $\mathcal{S}_h$. This, in general, are unrealistic. Let us see some examples.

Example 4.1. Consider a constant field $\mathbf{v}^0 = u^0\mathbf{i} + v^0\mathbf{j}$. The equations (4.2) have the solution $x = u^0 t + x_0$, $y = v^0 t + y_0$. Replacing it into (4.5) we get

$$\mathbf{R} = \mathbf{R} = t\mathbf{v}^0 + z\mathbf{k} + \mathbf{r}_0 \ , \quad \mathbf{r}_0 = x_0\mathbf{i} + y_0\mathbf{j}, \ \ z = h(x, y) + z_0 - h(x_0, y_0)$$

The is the equation of a vertical plane and we see that the streamlines of $\mathbf{U}^0$ are obtained by moving vertically the curve defined by the intersection of plane $\mathbf{R}$ with the topography. In other words, the shape of streamlines is the same for any z_0. This behavior is unrealistic since the terrain effects decrease as z_0 increases, in such manner that the streamlines tend to horizontal lines rather than follow the terrain.

Example 4.2. Consider $\mathbf{v}^0 = \beta x\mathbf{i} + \beta y\mathbf{j}$ with constant β. The Eq. (4.2) yields $x = x_0 e^{-\beta t}$, $y = y_0 e^{-\beta t}$ and Eq. (4.4) yields the equation of a plane $\mathbf{R} = x(\mathbf{i} + y_0/x_0\mathbf{j}) + z\mathbf{k}$. Equation (4.3) takes the form $\dot{z} = \dot{h} - 2\beta\sigma$ and yields $z = h(x, y) + [z_0 - h(x_0, y_0)]\, e^{-2\beta t}$, so that the streamlines of $\mathbf{U}^0$ converge asymptotically toward the topography for $\beta > 0$.

The examples show that the surface $\mathbf{R}(t, z, x_0, y_0)$ contains the streamlines of $\mathbf{U}^0$ for the same condition (x_0, y_0). The field $\mathbf{v}_{mnl}$ has similar behavior for small S_3 since $\mathbf{U}^0$ is a limiting case of $\mathbf{v}_{mnl}$ as $S_3 \to 0$ [Eq. (2.12)]. The proof is based on the following asymptotic expression

$$\dot{x} = u^0(x, y) + S_3 \mathrm{O}(S_3; x, y, \sigma) \ , \qquad \dot{y} = v^0(x, y) + S_3 \mathrm{O}(S_3; x, y, \sigma) \tag{4.6}$$

These equations are coupled with the vertical coordinate z because of the terms with S_3, so that in general streamlines with the same condition (x_0, y_0) do not belong to the surface $\mathbf{R}(t, z, x_0, y_0)$. As is shown below, this coupling can be used to generate a more realistic flow.

Small values of S_3 yield unphysical fields $\mathbf{v}_{mn}$, which are basically equal to $\mathbf{U}^0$, since the behavior of streamlines on the terrain is almost the same for larger z values. The examples of section 3 show that the effect of the terrain on $\mathbf{v}_{mn}$ can be adjusted with values S_3 of order 1. This confirms the

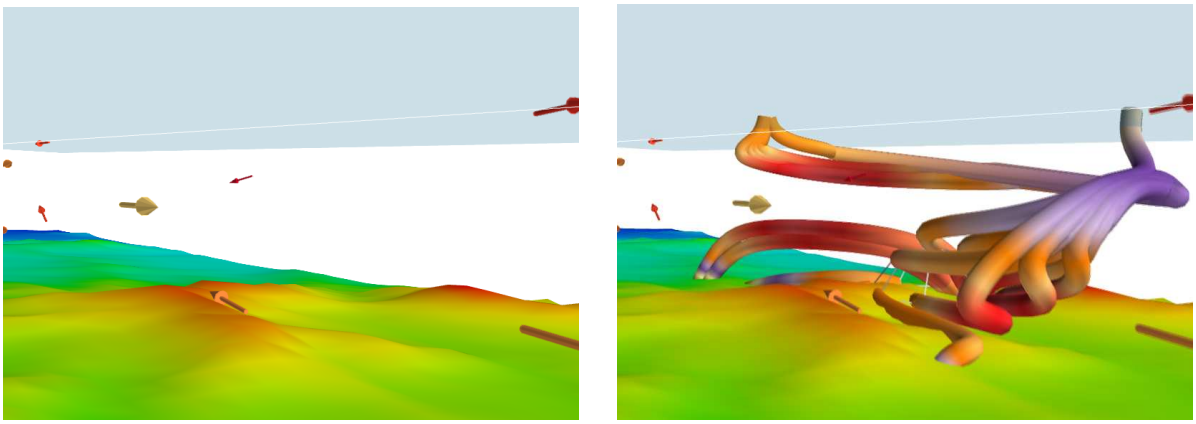

(a) **(b)**

Figure 6: a). The resulting mass conservative boundary layer wind field over the Ajusco mountain in Mexico City. b). The wind current tubes, for the case in a).The discretized mesh being 100x100x6, with 60000 nodes in total.

convenience of using free parameters in matrix $\mathbb{S}$ to get more realistic fields, as was pointed out by other authors [5,6].

5. Accuracy of the mass balance

The main goal of the present method to compute a wind field, is to get a field that obey the mass-balance. To show that this is indeed the case, in this section we report the flow-rate in simple examples and the results are compared with values given by standard formulations [2,4-17]. Consider three-dimensional examples in a parallelepiped Ω with sides $x_M = y_M$, z_M, a flat terrain ($h = 0$) and the field

$$\mathbf{v}^0 = u^0\mathbf{i} \quad \text{with} \quad u^0 = \beta\ e\,(y)\ \ f(z)\ g(x), \quad xz$$

where β is a constant determined by the average velocity $\langle u^0 \rangle = |\Omega|^{-1} \int_\Omega u^0 d\Omega = 10\ \text{ms}^{-1}$, $|\Omega| = x_M y_M z_M$. Since in general the boundary value problem (2.8) has to be solved with approximations in the vertical coordinate, we consider the problem

$$L\lambda_{mnl} = F_{mnl} \quad \text{in } \Omega_\sigma, \qquad \mathcal{L}\lambda_{mnl} = \xi_{mnl} \quad \text{on } \Gamma_\sigma\ ,$$

where λ_{mnl}, F_{mnl}, ξ_{mnl}, are Fourier series of λ, $F \equiv \nabla \cdot \mathbf{v}^0$, $\mathbf{n}_\sigma \cdot (\mathbf{U}^{0\eta} - \mathbf{v}^{0\eta})$ on Γ_σ, with the eigenfunctions of operator L subject to Neumann boundary conditions. The corresponding field is

$$\mathbf{v}_{mnl} = \mathbf{v}^0 + \mathbb{S}^{-1}\nabla\lambda_{mnl}\ .$$

We have $F = \beta e f \partial_x g$, $F_{mnl} = \beta e_n f_l \dot{g}_m$, where

$$e_n = \sum_{j=1}^{n} g_{yj}\phi_j\ , \quad f_l = \sum_{k=1}^{l} f_k\phi_k\ , \quad \dot{g}_m = \sum_{i=1}^{m} \dot{g}_i\phi_i,$$

are the Fourier series of g_y, f and $\partial_x g$, respectively. The accuracy with which $\mathbf{v}_{mnl}$ satisfies the continuity equation is given by

$$\nabla \cdot \mathbf{v}_{mnl} = F - F_{mnl} = \beta\,(\ e\ f\ \partial_x g - e_n\ f_l\ \dot{g}_m)\ .$$

Instead of computing $\nabla \cdot \mathbf{v}_{ml}$ point–by-point, we report the flux

$$\mathcal{F}\,(\Gamma^*, \mathbf{v}_{mnl}) = \int_{\Gamma^*} \mathbf{v}_{mnl} \cdot \mathbf{n}\ ds$$

in a region $\Omega^* = (a,b)^2 \times (c,d)$ with boundary Γ^*. From a computational and theoretical point of view, the flow-rate is a convenient quantity to compute the accuracy with which $\mathbf{v}_{mnl}$ satisfies the equation of continuity. In fact, the Schwarz inequality yields

$$|\mathcal{F}(\Gamma^*, \mathbf{v}_{mnl})| = |\Omega^*| \times \|F - F_{mnl}\|_{\Omega^*}, \tag{5.16}$$

where $|\Omega^*|$ is the volume of region Ω^* and $\|\cdot\|_{\Omega^*}$ is the norm of the Hilbert space $L^2(\Omega)$. The completeness of eigenfunctions guarantees that the series F_{mnl} converges to F in norm, namely,

$$\|F - F_{mnl}\|_{\Omega^*} = \left[\int_{\Omega^*} (F - F_{mnl})^2 \; dxdydz\right]^{1/2} \quad \to \quad 0$$

as m, n, l, increase, so that we can compute a field $\mathbf{v}_{mnl}$ with a prescribed flow-rate.

In order to compare our proposal with standard formulations, we report values of the flow-rate given by fields $\mathbf{v}^1$, $\mathbf{v}^2$, which are define as follows. $\mathbf{v}^1$ minimizes $J(\mathbf{v}^1)$ subject to $\mathbf{n}\cdot\mathbf{v} = 0$ on $z = 0$. The field is $\mathbf{v}^1 = \mathbf{v}^0 + \mathbb{S}^{-1}\nabla\lambda^{(1)}$ where $\lambda^{(1)}$ is given by the most common elliptic problem considered in the literature to compute variational mass-consistent models [2,4-17], namely,

$$L\lambda^{(1)} = F\ , \quad \partial_z\lambda^{(1)}\Big|_{z=0} = 0\ , \quad \lambda^{(1)} = 0 \ \text{ on } \ x = 0, x_M,\, y = 0, y_M,\, z = z_M\ . \tag{5.1}$$

This problem is replaced by $L\lambda^{(1)}_{mnl} = F^{(1)}_{mnl}$ where $\lambda^{(1)}_{mnl}$, $F^{(1)}_{mnl}$, are series of the eigenfunctions of L subject to the boundary conditions (5.1). The resulting field is $\mathbf{v}^1_{mnl} = \mathbf{v}^0 + \mathbb{S}^{-1}\nabla\lambda^{(1)}_{mnl}$.

The second field $\mathbf{v}^2$ minimizes $J(\mathbf{v}^2)$ subject to $\mathbf{n}\cdot\mathbf{v}^2 = \mathbf{n}\cdot\mathbf{U}^0$ on $x = 0, x_M$, $y = 0, y_M$, $z = 0$. The field is $\mathbf{v}^2 = \mathbf{v}^0 + \mathbb{S}^{-1}\nabla\lambda^{(2)}$ where $\lambda^{(2)}$ is given by the problem

$$L\lambda^{(2)} = F\ , \quad \partial_z\lambda^{(2)}\Big|_{z=0} = \partial_x\lambda^{(2)}\Big|_{x=0,x_M} = \partial_y\lambda^{(2)}\Big|_{y=0,y_M} = 0\ , \quad \lambda^{(2)} = 0 \text{ on } \ z = z_M\ . \tag{5.2}$$

This problem is replaced by $L\lambda^{(2)}_{mnl} = F^{(2)}_{mnl}$ where $\lambda^{(2)}_{mnl}$, $F^{(2)}_{mnl}$, are series of the eigenfunctions of L subject to the boundary conditions (5.1). The resulting field is $\mathbf{v}^2_{mnl} = \mathbf{v}^0 + \mathbb{S}^{-1}\nabla\lambda^{(2)}_{mnl}$.

Table I shows that the values $\mathcal{F}(\Gamma^*, \mathbf{v}_{mnl})$ given by our proposal are exactly zero, in contrast, the values given by standard approaches $\mathcal{F}\left(\Gamma^*, \mathbf{v}^{i=1,2}_{mnl}\right)$ are non zero and increase rapidly as Γ^* tends to the boundary Γ of region Ω. In Table II, the values $\mathcal{F}(\Gamma^*, \mathbf{v}_{mnl})$ are lower than $\mathcal{F}\left(\Gamma^*, \mathbf{v}^{i=1,2}_{mnl}\right)$ for interior regions and tend to the machine's floating point zero $\Gamma^* \to \Gamma$ whereas the values from $\mathbf{v}^{i=1,2}_{mnl}$ increase rapidly. These results show that our approach is indeed reliable to compute mass-consistent wind fields.

TABLE I. Flux $\mathcal{F}(\Gamma^*, \mathbf{v}_{m=n=l=50})$ in $\mathrm{km^3 s^{-1}}$ for $\mathbf{v}^0 = \beta xz\mathbf{i}$.

$\mathbf{w}_{mnl} \setminus \Omega_i$	$(8,\,12)^2\times(2,\,3)$	$(4,\,16)^2\times(1,4)$	$(0,\,20)^2\times(0,\,5)$
$\mathbf{v}_{mnl}$	zero	zero	zero
$\mathbf{v}^1_{mnl}$	6×10^{-7}	3×10^{-5}	5×10^{-2}
$\mathbf{v}^2_{mnl}$	2×10^{-7}	1×10^{-5}	2×10^{-2}

TABLE II. Flux $\mathcal{F}(\Gamma^*, \mathbf{v}_{m=n=l=50})$ in $\mathrm{s^{-1}}$ for $u^0 = \beta z\cos\omega x$, $\omega = \pi/2x_M$.

$\mathbf{w}_{mnl} \setminus \Omega_i$	$(8,\,12)^2\times(2,\,3)$	$(4,\,16)^2\times(1,4)$	$(0,\,20)^2\times(0,\,5)$
$\mathbf{v}_{mnl}$	-2×10^{-8}	-6×10^{-7}	zero
$\mathbf{v}^1_{mnl}$	-4×10^{-7}	-3×10^{-5}	-4×10^{-2}
$\mathbf{v}^2_{mnl}$	-2×10^{-7}	-1×10^{-5}	-1×10^{-2}

More theoretical and numerical results about the effect of boundary conditions in VMCM's are given in Refs. [18,19,21,22].

6. Conclusions

We have seen a formulation to compute VMCMs, which has the following features: (i) It leads to a separable elliptic equation which can be solved by means of eigenfunction expansions independently of the complexity of the terrain. This reduces the computational problem to the use of 2D and 3D Fast Fourier Algorithm (FFT), for which there are highly efficient computational routines. (ii) The scheme yields an explicit expression of the accuracy of the wind field to satisfy the continuity equation, expression that requires only the estimation of a three-dimensional Fourier Series. (iii) The imposed boundary conditions are easy to use and improve in several orders of magnitude the accuracy with which velocity field satisfies the continuity equation. In meteorology, one of the methods used to estimate the vertical velocity from a smooth field $\mathbf{v}^0$ (2.17a), is the estimation of $\mathbf{U}^0$ (2.17) or a similar one [20]. We saw that $\mathbf{U}^0$ may be unrealistic since the behavior of its streamlines can be the same at any height.

References

[1] Trenberth, K. E., J. W. Hurrell, A. Solomon, "Conservation of mass in three dimensions in global analyses", *J. Climate* **8**, 692–708.

[2] D. W. Byun, "Dynamically Consistent Formulations in Meteorological and Air Quality Models for Multiscale Atmospheric Studies. Part II: Mass Conservation Issues", *J. Atmos. Scien.* **56**, 3808 (1999).

[3] R. Daley, *Atmospheric data analysis* (Cambridge University Press, New York, 1991).

[4] Y. Sasaki, *J. Met. Soc. Japan* **36**, 77–88 (1958); *Mont. Wea. Rev.* **98**, 875-883 (1970).

[5] C.F. Ratto, R. Festa, C. Romeo, O.A. Frumento and M. Galluzzi, "Mass-consistent models for wind fields over complex terrain: The state of the art", *Environ. Software* **9**, 247-268 (1994).

[6] G. F. Homicz, *Three-Dimensional Wind Field Modeling: A Review*, Sandia National Laboratories, report SAN2002-2597 (2002).

[7] Guo, X. and Palutikof, J. P., "A Study of Two Mass-Consistent Models: Problems and Possible Solutions", *Bound.-Layer Meteor.* **53**, 303-332 (1990).

[8] Davis, C. G., Bunker, S. S. and Mutschlecner, J. P. "Atmospheric Transport Models for Complex Terrain", *Journal of Climate and Applied Meteorology* **23**, 235-238 (1984).

[9] T. Kitada, K. Igarashi, M. Owada, "Numerical analysis of the air pollution in a combined field of land/sea breese and the mountain/valley wind" *J. Climate Appl. Met.* **25**, 767-784 (1986).

[10] Ishikawa, H., "Mass-Consistent Wind Model as a Meteorological Preprocessor for Tracer Transport Models", *J. Appl. Meteorol.* **33**, 733-743 (1994).

[11] Y. Wang, C. Williamson, D. Garvey, S. Chang, J. Cogan, "Application of a Multigrid Method to a Mass-Consistent Diagnostic Wind Model", *J. Appl. Meteorol.* **44**, 1078 (2005).

[12] N. Sanín, G. Montero, "A finite difference model for air pollution simulation, *Adv. in Engineering Software* **38**, 358–365 (2007).

[13] D. Carstoiu, V. E. Oltean, G. Gorghiu, A. Olteanu, A. Cernian, "Approaches in wind modeling and air quality monitoring systems", *Bulletin UASVM, Horticulture* **65**(2), 1843–5394 (2008).

[14] M.A. Núñez, C. Flores, H. Juárez, *J. Comput. Met. Sci. Eng.* **7**, 21-42 (2007).

[15] C. Flores, H. Juárez, M. A. Núñez, M. L. Sandoval, *Num. Methods Partial Differential Equations* **26**, 826 (2010).

[16] S. Finardi, G. Tinarelli, A. Nanni, G. Brusasca, G. Carboni, "Evaluation of a 3–D flow and pollutant dispersion modelling system to estimate climatological ground level concentrations in complex coastal sites", *Int. J. Environ. Pollution* **16**, 472–482 (2001).

[17] F. Castino, L. Rusca, G. Solari, "Wind climate micro–zoning: a pilot application to Liguria Region (North–Western Italy)", *J. Wind Eng. Ind. Aerodynam.* **91**, 1353–1375 (2003).

[18] M. A. Núñez, "New scheme to compute mass–consistent models of geophysical flows", in "Proceedings of the I Workshop on Asymptotics for Parabolic and Hyperbolic Systems", Laboratóiro Nacional de Computação Científica, Petrópolis-R. J., Brasil (2008).

[19] M.A. Núñez, J. E. Sanchez Sanchez, "A formulation to compute mass-consistent models of hydrodynamic flows", submitted.

[20] J. Holton, *An introduction to Dynamic Meteorology* (Academic Press, San Diego, 1992), Sec. 3.5. T. N. Krishnamirti, *An introduction to Numerical Weather Prediction Techniques* (CRC Press, Boca Raton, 1996), Chap. 3.

[21] M.A. Núñez, "Improving variational mass-consistent models of hydrodynamic flows via boundary conditions", submitted.

[22] M.A. Núñez, C. Flores, H. Juárez, "A study of hydrodynamic mass consistent models", *J. Comput. Met. Sci. Eng.* **6**, 365-385 (2006).